iScience

CellPress
OPEN ACCESS

Article

Highly active manganese nitride-europium nitride catalyst for ammonia synthesis

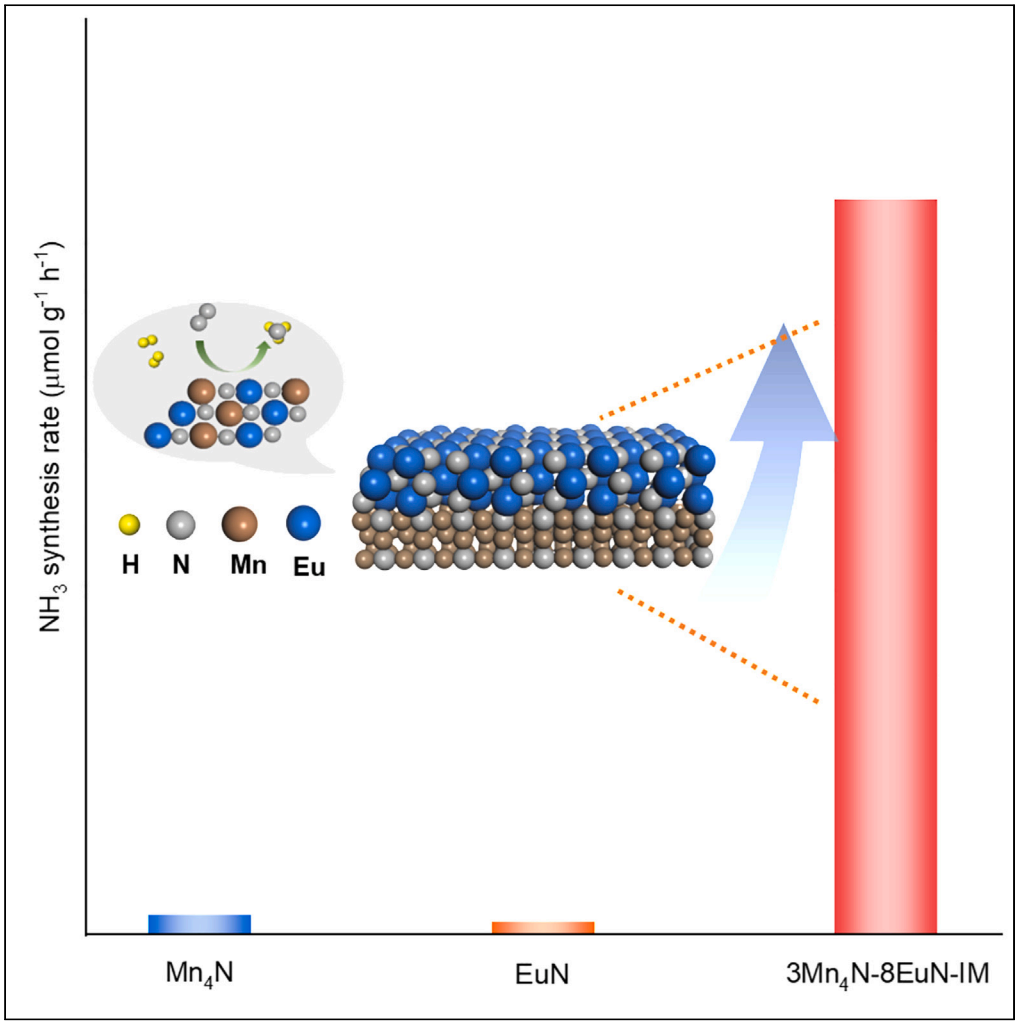

Jiemin Wang, Lin Liu, Ruili Li, ..., Teng He, Jianping Guo, Ping Chen

liulin@dicp.ac.cn (L.L.)
guojianping@dicp.ac.cn (J.G.)

Highlights

Mn_4N-EuN shows a much better activity than Mn_4N and EuN alone

The proximity of Mn_4N and EuN greatly affects the activity of the composite catalyst

The [Eu-N-Mn] interface structure is crucial for ammonia synthesis

Combining other rare earth nitrides with Mn_4N also leads to a dramatic increase in activity

Wang et al., iScience 27, 110858
September 20, 2024
https://doi.org/10.1016/j.isci.2024.110858

iScience

CellPress
OPEN ACCESS

Article

Highly active manganese nitride-europium nitride catalyst for ammonia synthesis

Jiemin Wang,[1,2] Lin Liu,[2,3,*] Ruili Li,[2,4] Shangshang Wang,[2,3] Xiaohua Ju,[2] Teng He,[2,3] Jianping Guo,[2,3,5,*] and Ping Chen[2,3]

SUMMARY

The development of efficient catalysts for ammonia synthesis under mild conditions is critical for establishing a carbon-neutral society powered by renewable ammonia. While significant effort has been focused on Fe and Ru-based catalysts, there have been very limited studies on manganese-based catalysts for ammonia synthesis because of their low intrinsic catalytic activity. Herein, we report that the synergy between manganese nitride (Mn_4N) and europium nitride (EuN) yields an ammonia synthesis rate that is 41 and 25 times higher than that of neat Mn_4N and EuN, respectively. Detailed studies suggest that a [Eu-N-Mn] species at the interface of Mn_4N and EuN plays a pivotal role in ammonia synthesis. Compositing of Mn_4N with other rare earth metal nitrides such as LaN, PrN, and CeN also leads to a significant enhancement in catalytic activity. This work broadens the scope of advanced nitride catalysts for ammonia synthesis.

INTRODUCTION

Ammonia synthesis from nitrogen and hydrogen via Haber-Bosch process is one of the most important chemical industrial processes in the world.[1] With the increasing concerns on the energy consumption of ammonia synthesis process, developing more efficient catalysts has attracted much attention from both academia and industry. However, catalytic ammonia synthesis under mild conditions remains challenging due to the inert chemical nature of dinitrogen molecules.[2] As yet, most studies about ammonia synthesis have been focused on supported Ru metal and fused iron catalysts.[3–6] Recently, intermetallic compounds,[7,8] metal carbides,[9] metal nitrides,[10–12] transition metal-alkali (or alkaline earth) metal hydride composites,[13,14] and oxyhydride supported metals have also been found to be efficient catalysts for ammonia synthesis typically under low temperatures and pressures.[15–17]

Transition metal nitrides (TMNs) have been widely studied in catalysis because of their noble metal-like catalytic properties.[18] Up to now, a variety of TMNs based on earth-abundant metals (Mo_2N, Co_3Mo_3N, Fe_3Mo_3N, and Ni_2Mo_3N etc.) have been investigated in ammonia synthesis.[19–24] Usually, binary metal nitrides such as Mo_2N have limited activities toward ammonia synthesis even under harsh reaction conditions. Compared with binary metal nitrides, ternary metal nitrides such as Co_3Mo_3N have been found to exhibit much better catalytic performances in ammonia synthesis,[20,21] which is considered to be closely associated with suitable nitrogen binding energy of the Co-Mo bimetallic catalyst.[25] Although encouraging progress has been made for developing metal nitride catalysts by adjusting their structures, compositions and preparation methods, strategies for designing new kinds of effective metal nitride catalysts are still highly desirable.[18,26]

A heterostructure is expected to have a large diversity of shapes, compositions, and especially interfaces, as each of its domains can be tuned,[27] whereby its functionality changes according to the different components in the structure. Chen et al. showed that the catalytic activities of transition metals (TM)/TMN can be significantly enhanced with the addition of alkali or alkaline earth metal hydride.[13,14] The effect of alkali or alkaline earth metal hydride is more prominent on the nitrides of V, Cr, and Mn. Nanoscale metal-metal nitride interfaces have been reported to display advantages in heterogeneous catalysis owing to their flexibility of structures and compositions. For instance, rare earth metal nitrides (LnN) supported transition metal catalysts (Ni/LaN and Ni/CeN) have been demonstrated to be effective catalysts for ammonia synthesis reaction.[28–30] The abundant metal-metal nitride interface of TM/LnN catalysts is believed to play a vital role in activating N_2 and ammonia synthesis due to the presence of abundant surface N vacancy species and unique electronic structures.

Rational design of the metal nitride-based catalysts with abundant interface structure might thus help us to obtain catalysts with good activity for ammonia synthesis reaction. Inspired by the strategy of constructing interfacial active centers in multifunctional heterogeneous catalyst systems, we therefore try to cooperate two kinds of metal nitrides with controlled interfacial architecture to develop efficient

[1]School of Chemistry, Dalian University of Technology, Dalian 116024, P.R. China
[2]Dalian Institute of Chemical Physics, Chinese Academy of Sciences, Dalian 116023, P.R. China
[3]Center of Materials Science and Optoelectronics Engineering, University of Chinese Academy of Sciences, Beijing 100049, P.R. China
[4]Department of Chemical Physics, University of Science and Technology of China, Hefei 230026, P.R. China
[5]Lead contact
*Correspondence: liulin@dicp.ac.cn (L.L.), guojianping@dicp.ac.cn (J.G.)
https://doi.org/10.1016/j.isci.2024.110858

composite catalysts for ammonia synthesis reaction. Herein, we report a metal nitride composite catalyst composed of Mn_4N and EuN particles, which preserves the bulk structure of Mn_4N and EuN but shows superior catalytic activities to both of the single component in ammonia synthesis. The synergistic effect may originate from the formation of abundant interfacial active sites between the Mn_4N and EuN particles, which facilitating the activation and dissociation of N_2. Tuning the proximity of nitride particles in Mn_4N-EuN composite catalyst by adopting different preparation methods not only changes its catalytic performance in ammonia synthesis, but also demonstrates the key criterion of creating active sites in the interfacial region between two kinds of nitride particles.

RESULTS AND DISCUSSION

Catalytic performance and kinetic analyses

Here, we used EuH_2 and MnN as the precursors of Eu and Mn, respectively, to prepare the Eu-Mn composite catalysts. As shown in Figure S1, EuH_2 and MnN converted into EuN and Mn_4N, respectively, after the catalytic test. Figure 1A shows that Mn_4N and EuN alone show very low activities under 1.0 MPa below 450°C. Upon combination of Mn_4N with EuN by a simple ball milling method, the ammonia synthesis rates of Mn_4N-EuN composite catalysts are significantly enhanced (Figure S2). The highest activity was obtained for the Mn_4N-EuN sample with the molar ratio of Mn_4N/EuN = 3/8 (which is denoted hereafter as $3Mn_4N$-8EuN) (Figure 1A). The catalyst shows an apparent activity starting from 300°C (Figure 1B), and the ammonia synthesis rate at 450°C reaches 11,250 μmol g^{-1} h^{-1}, which is 41 and 25 times of that of the Mn_4N (270 μmol g^{-1} h^{-1}) and EuN (450 μmol g^{-1} h^{-1}), respectively. And we also found that the enhancement in activity is not caused by variations in specific surface area (see Table S1). By using an impregnation method, the performance of $3Mn_4N$-8EuN-IM can be further improved (Figure 1B), i.e., an NH_3 synthesis rate of 1,710 μmol g^{-1} h^{-1} was achieved at 300°C, which is 2.7 times of the ball milled $3Mn_4N$-8EuN sample, and even comparable to the benchmark Cs-Ru/MgO (1,386 μmol g^{-1} h^{-1}) under the same conditions (Figure 1B).[14] It is worthy of noting that the activity of Mn_4N-EuN catalyst is comparable to many active catalysts based on group VIII metals reported in literatures (Table S2). Considering the low activities of Mn_4N and EuN, the unexpected high activity of $3Mn_4N$-8EuN indicates the presence of synergistic effect of Mn_4N and EuN for ammonia synthesis.

The stability test of $3Mn_4N$-8EuN in ammonia synthesis was performed at 450°C (Figure S3A). The result shows that the activity of $3Mn_4N$-8EuN composite catalyst decreased slightly from 12,600 to 11,250 μmol g^{-1} h^{-1} within 10 h, which may be due to the agglomeration of catalyst during reaction. As shown in Figures S3B and S3C, the stability can be improved by mixing the Mn_4N-EuN composite with MgO powder. Specifically, the ammonia synthesis rate remained stable in a time period of 140 h at the conditions of 400°C and 1 MPa.

Kinetic analysis was conducted to study the reaction mechanism of ammonia synthesis over Mn_4N-EuN catalyst. Figures 1C and S4 present Arrhenius plots for ammonia synthesis reaction over xMn_4N-EuN composite catalysts with different Mn/Eu molar ratios. The $3Mn_4N$-8EuN catalyst has an apparent activation energy (E_a) of 65 ± 2 kJ mol^{-1}, which is much lower than those of Ru/MgO (79 kJ mol^{-1}) and Cs-Ru/MgO (120 kJ mol^{-1}) catalysts,[3,31] and comparable to some of the recently reported catalysts such as Ru/C12A7:e^- (53.6 kJ mol^{-1}),[32] Fe-LiH (46.5 kJ mol^{-1}),[13] BaCrHN (50.1 kJ mol^{-1}),[33] and Ni/LaN (57.5 kJ mol^{-1}) (Table S3).[28] For the xMn_4N-EuN sample with Mn/Eu molar ratio in the range of 0.0625–8, relatively small E_a values in the range of 63–69 kJ mol^{-1} can be achieved (Figure S4). The similar E_a values of xMn_4N-EuN catalysts suggest similar structure of the active sites in the different composites. The N_2 reaction order (β) of the $3Mn_4N$-8EuN sample is 1.34, suggesting that N_2 dissociation does control the overall reaction rate of ammonia synthesis (Figure 1D).[34,35] Previous studies have shown that the H_2 reaction order of traditional Ru-based catalysts is generally negative, which represents redundant adsorption of H_2 on the surface and thereby decreases the overall catalytic rate.[16,36] Notably, the H_2 reaction order of the $3Mn_4N$-8EuN sample is 1.68 (Figure 1D). This phenomenon is also reflected in the monotonic increase of NH_3 synthesis rates with the rise of reaction pressure (Figure S5), i.e., with the reaction pressure increased from 0.1 MPa to 1.0 MPa, the activity at 400°C shows a remarkable increase from 1080 to 6030 μmol g^{-1} h^{-1}. The NH_3 reaction order of $3Mn_4N$-8EuN, on the other hand, is −1.19 (Figure S6), revealing that NH_x (x = 1–3) species strongly bind on the catalyst surface. These kinetic analyses reveal that the catalyst would work well when N_2 and H_2 partial pressures are high and NH_3 partial pressure is low.

Structural characterization of Mn_4N-EuN catalyst

To understand the role of Mn_4N and EuN in ammonia synthesis, a series of control experiments were performed. As shown in Figure 2A, the activity of a sample for which Mn_4N and EuN were separated by quartz wool (630 μmol g^{-1} h^{-1}) is close to EuN (450 μmol g^{-1} h^{-1}) or Mn_4N (270 μmol g^{-1} h^{-1}). However, placing Mn_4N layer on top or beneath EuN layer leads to a considerably higher activity. We further examined the activity by regulating the contact degree of the two components in Mn_4N-EuN composite. It is interesting, though, that even the very gentle physical mixing of Mn_4N and EuN with a spatula provides efficient interaction between the two components, as the catalytic activity of the $3Mn_4N$-8EuN-S sample is even higher (5,850 μmol g^{-1} h^{-1}). Further increasing the contact of the two components by ball milling shows an obvious activity increase (11,250 μmol g^{-1} h^{-1}). These results clearly show that the closer intimacy of Mn_4N and EuN particles results in the better catalytic activity.

Based on these experimental observations, we supposed that some active species may be formed at the interface between Mn_4N and EuN during reaction, denoted as [Eu-N-Mn]. Although there are no reports about ternary nitrides of Eu and Mn, other nitrides of rare earth metal and transition metal such as $La_3V_2N_6$ and Ce_2MnN_3 have been synthesized under harsh reaction conditions,[37–39] and it might be possible to form [Eu-N-Mn] species under ammonia synthesis reaction conditions.

The spent Mn_4N-EuN composite catalyst was then subjected to X-Ray Diffraction (XRD), transmission electron microscopy (TEM), and X-ray photoelectron spectroscopy (XPS) characterizations for obtaining detailed structural information. The XRD patterns (Figure S7) show

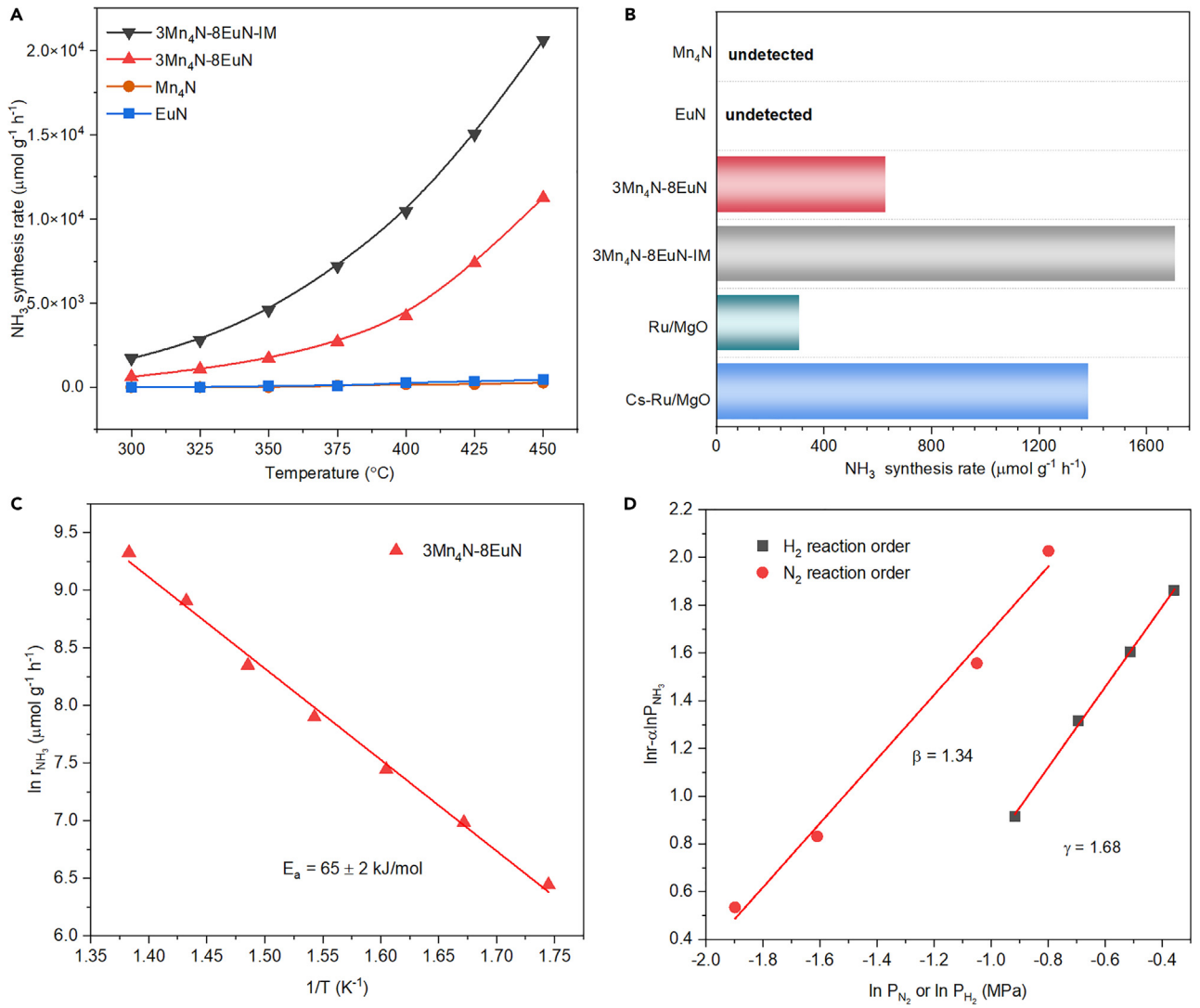

Figure 1. Catalytic performance of Mn_4N-EuN

(A) Ammonia synthesis rates of $3Mn_4N$-8EuN, $3Mn_4N$-8EuN-IM, Mn_4N, and EuN catalysts as a function of temperature under 1.0 MPa with the weight hourly space velocity (WHSV) of 60,000 mL g^{-1} h^{-1}.

(B) Ammonia synthesis rates of $3Mn_4N$-8EuN-IM, Mn_4N, EuN, Ru/MgO, and Cs-Ru/MgO catalysts at 300°C, 1.0 MPa, WHSV of 60,000 mL g^{-1} h^{-1}.

(C) Arrhenius plots for ammonia synthesis on $3Mn_4N$-8EuN under 1.0 MPa.

(D) H_2 (γ) and N_2 (β) reaction orders for the $3Mn_4N$-8EuN+MgO catalyst at 400°C and 1.0 MPa.

Mn_4N and EuN are the only observed crystalline phases. From TEM images (Figures 2B and S8), the lattice fringes attributable to Mn_4N(111) and EuN(200) can be observed. XPS (Figure 2C) shows that the binding energy of 396 eV can be attributed to the Mn-N bond, and the value of 399 eV might be ascribed to the adsorbed NH_x (x = 1 and 2).[40] We also noted that, for the spent $3Mn_4N$-8EuN sample, the binding energy of Mn 2p shifted to a lower value, suggesting electron transfer from Eu to Mn because of their different electronegativities (1.55 and 1.2 for Mn and Eu, respectively). The morphology and distribution of elements were characterized by Scanning Electron Microscope Energy-Dispersive X-ray Spectroscopy (SEM-EDX) (Figure S9). Combined with TEM results, the catalyst is composed of many small particles. And Eu, N and Mn were distributed in the same area at the micron scale, meaning that the Mn, N and Eu elements on the catalyst surface are uniformly distributed. To further explore the reaction mechanism, we conducted H_2-TPR-MS on the catalysts after testing. The $3Mn_4N$-8EuN, EuN, and Mn_4N samples were tested at 450°C for 5 h, then cooled to room temperature in the reaction atmosphere, and then switched to pure H_2. As shown in Figure 3A, the tested EuN shows one weak ammonia peak between 300°C and 500°C, while there is no obvious ammonia peak for the tested Mn_4N. Different from that of the Mn_4N and EuN, a weak peak around 175°C and a very broad and strong peak between 350°C and 600°C can be observed in the H_2-TPR profile of $3Mn_4N$-8EuN sample. The presence of such strong peak evidences the formation of new kind of N species in the $3Mn_4N$-8EuN composite, which have higher reactivity toward

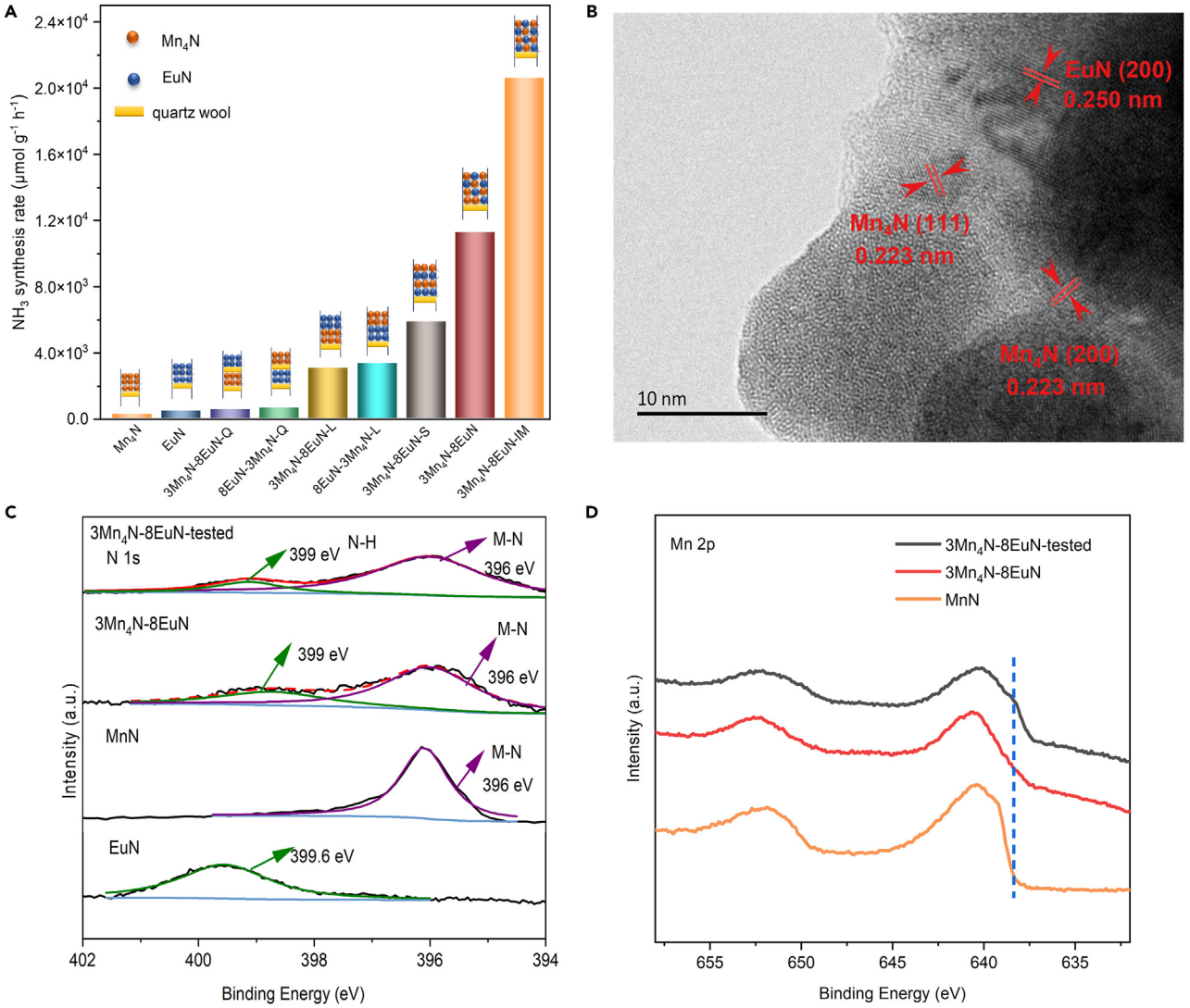

Figure 2. Structural characterization of Mn_4N-EuN catalyst

(A) Effect of contact between Mn_4N and EuN on catalyst activity. Reaction conditions: 30 mg catalyst, $3H_2/1N_2$ = 30 mL min^{-1}, 1.0 MPa.

(B) TEM images of $3Mn_4N$-8EuN collected after reaction.

(C) N 1s core level XPS spectra of $3Mn_4N$-8EuN, MnN, and EuN.

(D)Mn 2p core level XPS spectra of $3Mn_4N$-8EuN before and after reaction.

hydrogenation to NH_3. The H_2-TPR-MS results suggest that the nature of synergy of Mn_4N and EuN is to facilitate the formation of active N species in the $3Mn_4N$-8EuN composite, which are closely related with the formation of interfacial Eu-N-Mn structure at the interface region in the $3Mn_4N$-8EuN composite. And N_2 desorption from the used $3Mn_4N$-8EuN occurs above 480°C (Figure S10), which was not observed over Mn_4N and EuN. This result further supports the possible formation of active N species at the Mn_4N-EuN composite catalysts.

N_2 activation over Mn_4N-EuN catalyst

It is generally believed that ammonia synthesis from N_2 and H_2 molecules involves the adsorption and dissociation of surface N_2 and H_2 molecules, and the following hydrogenation of surface dissociated N atoms to NH_3 on the transition metal catalyst surfaces. Alternatively, the N vacancies on the surface of metal nitrides such as Co_3Mo_3N have been suggested as the active site for the activation of reactants and formation of NH_3 molecules.[10,41] To get more understanding on the reaction mechanism, the activation of N_2 over $3Mn_4N$-8EuN, Mn_4N, and EuN samples were investigated by N_2 isotope exchange experiment (Figure 3B). It can be seen that very weak signal of $^{29}N_2$ can be observed over neat Mn_4N and EuN samples, suggesting the weak activity of Mn_4N and EuN for activating and dissociating $^{28}N_2$ and $^{30}N_2$. Under identical conditions, obvious $^{28}N_2/^{30}N_2$ exchange reaction occurred on the $3Mn_4N$-8EuN composite at 400°C, leading to the formation of $^{29}N_2$ at the

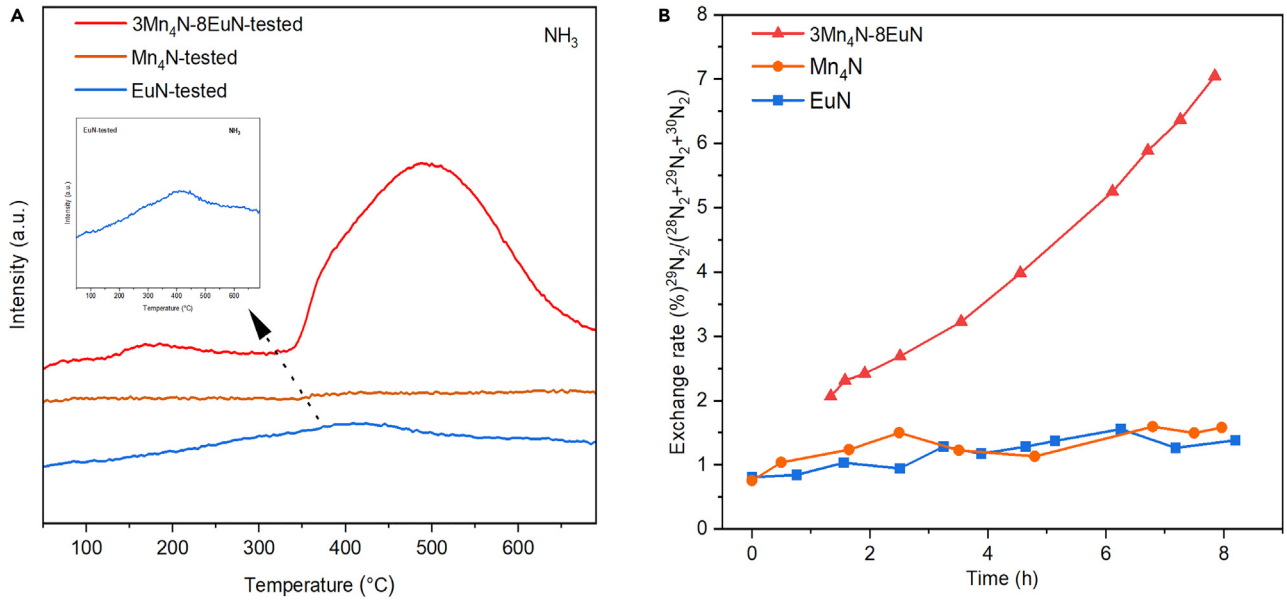

Figure 3. N_2 activation over Mn_4N-EuN catalyst

(A) H_2-TPR-MS profiles for the tested $3Mn_4N$-8EuN, Mn_4N, and EuN catalysts under a flow of pure H_2 at a ramping rate of 5 °C min^{-1}.

(B) N_2 isotope exchange rates of $3Mn_4N$-8EuN, Mn_4N, and EuN at 400°C under 32 kPa ($^{28}N_2$:$^{30}N_2$ = 4.4: 1).

expense of $^{28}N_2$ and $^{30}N_2$. Compared with that of the Mn_4N and EuN samples, the high $^{28}N_2/^{30}N_2$ exchange rate clearly demonstrates the strong capability of $3Mn_4N$-8EuN composite for activation and dissociation of N_2 molecules.

Based on these experimental results, we propose that an active [Eu-N-Mn] species at the surface or interface of Mn_4N-EuN composite catalysts might be formed during the reaction, and the N in [Eu-N-Mn] can react facilely with H_2 to form NH_3 and N vacancy sites. N_2 molecules are then adsorbed and activated at N vacancy sites to form the [Eu-N-Mn] to complete the catalytic cycle.

Performance of other Mn_4N-LnN catalysts

Based on the understanding of synergistic effect of Mn_4N with EuN, we then further investigated the catalytic performances of other Mn_4N-LnN composite catalysts for ammonia synthesis. Similar to the Mn_4N-EuN composite catalysts, the activities of Mn_4N-LnN composites show

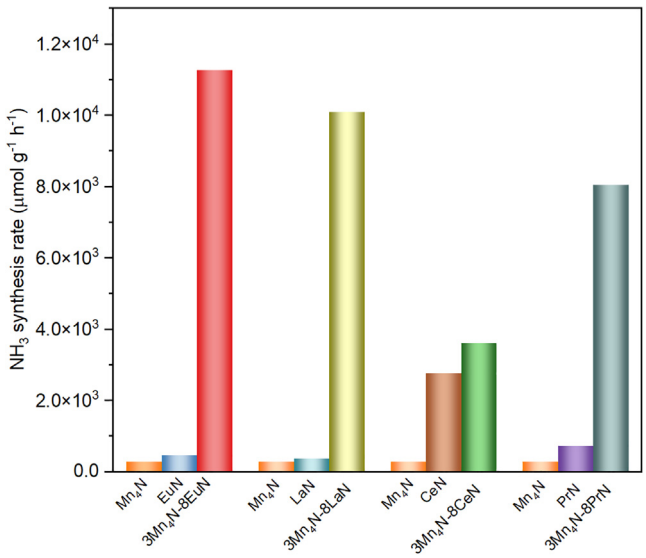

Figure 4. Ammonia synthesis rates of $3Mn_4N$-8EuN, $3Mn_4N$-8LaN, $3Mn_4N$-8CeN, $3Mn_4N$-8PrN, Mn_4N, and LnN under the reaction conditions of WHSV of 60,000 mL g_{cat}^{-1} h^{-1}, 1.0 MPa, and 450°C

a remarkable improvement as compared with those of the single nitride component alone under identical reaction conditions (Figure 4). Specifically, the $3Mn_4N-8LaN$ achieves an ammonia synthesis rate of 10,080 μmol g^{-1} h^{-1} at 450°C, which is ca. 37 and 28 times of that of Mn_4N and LaN (360 μmol g^{-1} h^{-1}), respectively. The PrN shows a low activity at 450°C (720 μmol g^{-1} h^{-1}), while an ammonia synthesis rate of 8,040 μmol g^{-1} h^{-1} can be achieved upon compositing with Mn_4N. The unprecedentedly improved activity suggests that Mn_4N can also react with LnN (PrN, CeN, and LaN) and likely form interfacial active [Ln-N-Mn] sites in the composite samples, which provides an energy favorable reaction pathway for ammonia synthesis reaction. The superior activity of Mn_4N-LnN composites further confirms the crucial role of interfacial active structure in ammonia synthesis, which offers a new strategy to design efficient ammonia synthesis composite catalysts based on earth-abundant metal nitrides.

Conclusion

In summary, we report an active Mn_4N-EuN composite catalyst for ammonia synthesis. The proximity of Mn_4N and EuN particles is a key factor in optimizing the performance of the catalyst. The formation of Eu-N-Mn species is critically important to understand the catalytic function of this composite nitride catalyst. The synergy of Mn_4N and rare earth metal nitrides has been found universal in different Mn_4N-LnN composite catalysts. The nature of interface of Mn nitride and rare earth metal nitride at the atomic level remains an open question, which needs advanced characterization techniques. The exploration of other nitride-based composite catalysts containing early transition metals and rare earth metals is worthy of future studies. By screening the proportions of early metals and rare earth metals, a nitride catalyst showing superior activity for ammonia synthesis under mild conditions to those of Fe and Ru could be developed.

Limitation of the study

Detailed information about the structure of the [Eu-N-Mn] interface remains elusive and requires more advanced characterization techniques.

RESOURCE AVAILABILITY

Lead contact

Further information and requests for resources should be directed to and will be fulfilled by the lead contact, Jianping Guo (guojianping@dicp.ac.cn).

Materials availability

This study did not generate new unique reagents.

Data and code availability

- Data reported in this paper will be shared by the lead contact upon request.
- This paper does not report original code.
- Any additional information required to reanalyze the data reported in this paper is available from the lead contact upon request.

ACKNOWLEDGMENTS

We acknowledge the financial support from the National Key Research and Development Program of China (2021YFB4000400), National Natural Science Foundation of China (22179128 and 21988101), and Energy Revolution S&T Program of Yulin Innovation Institute of Clean Energy (E302102001).

AUTHOR CONTRIBUTIONS

J.G., L.L., and P.C. supervised the project and revised the paper. J.W. conducted the most experiments and wrote the paper. R.L. conducted some of experiments. S.W. provided part of the sample preparation methods. X.J. and T.H. analyzed some experiment results. All authors discussed the results and commented on the manuscript at all stages.

DECLARATION OF INTERESTS

A patent application (202311567625.1) has been filed with the China National Intellectual Property Administration.

STAR★METHODS

Detailed methods are provided in the online version of this paper and include the following:

SUPPLEMENTAL INFORMATION

Supplemental information can be found online at https://doi.org/10.1016/j.isci.2024.110858.

Received: May 29, 2024
Revised: July 9, 2024
Accepted: August 28, 2024
Published: August 31, 2024

REFERENCES

1. Erisman, J.W., Sutton, M.A., Galloway, J., Klimont, Z., and Winiwarter, W. (2008). How a century of ammonia synthesis changed the world. Nat. Geosci. *1*, 636–639. https://doi.org/10.1038/ngeo325.
2. Jia, H.P., and Quadrelli, E.A. (2014). Mechanistic aspects of dinitrogen cleavage and hydrogenation to produce ammonia in catalysis and organometallic chemistry: relevance of metal hydride bonds and dihydrogen. Chem. Soc. Rev. *43*, 547–564. https://doi.org/10.1039/c3cs60206k.
3. Bielawa, H., Hinrichsen, O., Birkner, A., and Muhler, M. (2001). The ammonia-synthesis catalyst of the next generation: Barium-promoted oxide-supported ruthenium. Angew. Chem., Int. Ed. Engl. *40*, 1061–1063. https://doi.org/10.1002/1521-3773(20010316)40:6<1061::AID-ANIE10610>3.0.CO;2-B.
4. Liang, C., Li, Z., Qiu, J., and Li, C. (2002). Graphitic nanofilaments as novel support of Ru-Ba catalysts for ammonia synthesis. J. Catal. *211*, 278–282. https://doi.org/10.1006/jcat.2002.3724.
5. Arabczyk, W., Narkiewicz, U., and Moszyński, D. (1996). Chlorine as a poison of the fused iron catalyst for ammonia synthesis. Appl. Catal. Gen. *134*, 331–338. https://doi.org/10.1016/0926-860x(95)00211-1.
6. Kalenczuk, R.J. (2000). Cobalt promoted fused iron catalyst for ammonia synthesis. Int. J. Inorg. Mater. *2*, 233–239. https://doi.org/10.1016/s1466-6049(00)00009-x.
7. Wu, J., Gong, Y., Inoshita, T., Fredrickson, D.C., Wang, J., Lu, Y., Kitano, M., and Hosono, H. (2017). Tiered Electron Anions in Multiple Voids of LaScSi and Their Applications to Ammonia Synthesis. Adv. Mater. *29*, 1700924. https://doi.org/10.1002/adma.201700924.
8. Gong, Y., Wu, J., Kitano, M., Wang, J., Ye, T.N., Li, J., Kobayashi, Y., Kishida, K., Abe, H., Niwa, Y., et al. (2018). Ternary intermetallic LaCoSi as a catalyst for N_2 activation. Nat. Catal. *1*, 178–185. https://doi.org/10.1038/s41929-017-0022-0.
9. Kojima, R., and Aika, K.i. (2001). Molybdenum nitride and carbide catalysts for ammonia synthesis. Appl. Catal. Gen. *219*, 141–147. https://doi.org/10.1016/s0926-860x(01)00676-7.
10. Hunter, S.M., Gregory, D.H., Hargreaves, J.S.J., Richard, M., Duprez, D., and Bion, N. (2013). A study of $^{15}N/^{14}N$ isotopic exchange over cobalt molybdenum nitrides. ACS Catal. *3*, 1719–1725. https://doi.org/10.1021/cs400336z.
11. Zeinalipour-Yazdi, C.D. (2019). Mechanisms of ammonia and hydrazine synthesis on η-Mn_3N_2-(100) surfaces. Phys. Chem. Chem. Phys. *21*, 19365–19377. https://doi.org/10.1039/C9CP03934A.
12. Zeinalipour-Yazdi, C.D. (2018). On the possibility of an Eley–Rideal mechanism for ammonia synthesis on Mn6N5+x (x = 1)-(111) surfaces. Phys. Chem. Chem. Phys. *20*, 18729–18736. https://doi.org/10.1039/C8CP02381F.
13. Wang, P., Chang, F., Gao, W., Guo, J., Wu, G., He, T., and Chen, P. (2017). Breaking scaling relations to achieve low-temperature ammonia synthesis through LiH-mediated nitrogen transfer and hydrogenation. Nat. Chem. *9*, 64–70. https://doi.org/10.1038/nchem.2595.
14. Chang, F., Guan, Y., Chang, X., Guo, J., Wang, P., Gao, W., Wu, G., Zheng, J., Li, X., and Chen, P. (2018). Alkali and alkaline earth hydrides-driven N_2 activation and transformation over Mn nitride catalyst. J. Am. Chem. Soc. *140*, 14799–14806. https://doi.org/10.1021/jacs.8b08334.
15. Jiang, Y., Takashima, R., Nakao, T., Miyazaki, M., Lu, Y., Sasase, M., Niwa, Y., Abe, H., Kitano, M., and Hosono, H. (2023). Boosted activity of cobalt catalysts for ammonia synthesis with $BaAl_2O_{4-x}H_y$ electrides. J. Am. Chem. Soc. *145*, 10669–10680. https://doi.org/10.1021/jacs.3c01074.
16. Tang, Y., Kobayashi, Y., Masuda, N., Uchida, Y., Okamoto, H., Kageyama, T., Hosokawa, S., Loyer, F., Mitsuhara, K., Yamanaka, K., et al. (2018). Metal-Dependent Support Effects of Oxyhydride-Supported Ru, Fe, Co Catalysts for Ammonia Synthesis. Adv. Energy Mater. *8*, 1801772. https://doi.org/10.1002/aenm.201801772.
17. Ooya, K., Li, J., Fukui, K., Iimura, S., Nakao, T., Ogasawara, K., Sasase, M., Abe, H., Niwa, Y., Kitano, M., and Hosono, H. (2021). Ruthenium Catalysts Promoted by Lanthanide Oxyhydrides with High Hydride-Ion Mobility for Low-Temperature Ammonia Synthesis. Adv. Energy Mater. *11*, 2003723. https://doi.org/10.1002/aenm.202003723.
18. Hargreaves, J.S.J. (2013). Heterogeneous catalysis with metal nitrides. Coord. Chem. Rev. *257*, 2015–2031. https://doi.org/10.1016/j.ccr.2012.10.005.
19. Liu, N., Nie, L., Xue, N., Dong, H., Peng, L., Guo, X., and Ding, W. (2010). Catalytic Ammonia Synthesis over Mo Nitride/ZSM-5. ChemCatChem *2*, 167–174. https://doi.org/10.1002/cctc.200900155.
20. Kojima, R., and Aika, K.i. (2000). Cobalt molybdenum bimetallic nitride catalysts for ammonia synthesis. Chem. Lett. *29*, 514–515. https://doi.org/10.1246/cl.2000.514.
21. Jacobsen, C.J.H. (2000). Novel class of ammonia synthesis catalysts. Chem. Commun. *12*, 1057–1058. https://doi.org/10.1039/b002930k.
22. Hargreaves, J.S.J., and McKay, D. (2009). A comparison of the reactivity of lattice nitrogen in Co_3Mo_3N and Ni_2Mo_3N catalysts. J. Mol. Catal. Chem. *305*, 125–129. https://doi.org/10.1016/j.molcata.2008.08.006.
23. Higham, M.D., Zeinalipour-Yazdi, C.D., Hargreaves, J.S.J., and Catlow, C.R.A. (2023). Mechanism of ammonia synthesis on Fe_3Mo_3N. Faraday Discuss *243*, 77–96. https://doi.org/10.1039/d2fd00148a.
24. Zeinalipour-Yazdi, C.D. (2024). A Comparison of the Mechanisms and Activation Barriers for Ammonia Synthesis on Metal Nitrides (Ta3N5, Mn6N5, Fe3Mo3N, Co3Mo3N). Crystals *14*, 392.
25. Jacobsen, C.J., Dahl, S., Clausen, B.S., Bahn, S., Logadottir, A., and Nørskov, J.K. (2001). Catalyst design by interpolation in the periodic table: Bimetallic ammonia synthesis catalysts. J. Am. Chem. Soc. *123*, 8404–8405. https://doi.org/10.1021/ja010963d.
26. Mazumder, B., and Hector, A.L. (2009). Synthesis and applications of nanocrystalline nitride materials. J. Mater. Chem. *19*, 4673–4686. https://doi.org/10.1039/b817407e.
27. Wang, H., Fu, W., Yang, X., Huang, Z., Li, J., Zhang, H., and Wang, Y. (2020). Recent advancements in heterostructured interface engineering for hydrogen evolution reaction electrocatalysis. J. Mater. Chem. A Mater. *8*, 6926–6956. https://doi.org/10.1039/c9ta11646j.
28. Ye, T.N., Park, S.W., Lu, Y., Li, J., Sasase, M., Kitano, M., Tada, T., and Hosono, H. (2020). Vacancy-enabled N_2 activation for ammonia synthesis on an Ni-loaded catalyst. Nature *583*, 391–395. https://doi.org/10.1038/s41586-020-2464-9.
29. Ye, T.N., Park, S.W., Lu, Y., Li, J., Sasase, M., Kitano, M., and Hosono, H. (2020). Contribution of Nitrogen Vacancies to Ammonia Synthesis over Metal Nitride Catalysts. J. Am. Chem. Soc. *142*, 14374–14383. https://doi.org/10.1021/jacs.0c06624.
30. Zhang, K., Cao, A., Wandall, L.H., Vernieres, J., Kibsgaard, J., Nørskov, J.K., and Chorkendorff, I. (2024). Spin-mediated promotion of Co catalysts for ammonia synthesis. Science *383*, 1357–1363. https://doi.org/10.1126/science.adn0558.
31. Kitano, M., Inoue, Y., Ishikawa, H., Yamagata, K., Nakao, T., Tada, T., Matsuishi, S., Yokoyama, T., Hara, M., and Hosono, H. (2016). Essential role of hydride ion in ruthenium-based ammonia synthesis catalysts. Chem. Sci. *7*, 4036–4043. https://doi.org/10.1039/c6sc00767h.
32. Kitano, M., Inoue, Y., Yamazaki, Y., Hayashi, F., Kanbara, S., Matsuishi, S., Yokoyama, T., Kim, S.W., Hara, M., and Hosono, H. (2012). Ammonia synthesis using a stable electride as an electron donor and reversible hydrogen store. Nat. Chem. *4*, 934–940. https://doi.org/10.1038/nchem.1476.
33. Guan, Y., Zhang, W., Wang, Q., Weidenthaler, C., Wu, A., Gao, W., Pei, Q., Yan, H., Cui, J., Wu, H., et al. (2021). Barium chromium nitride-hydride for ammonia synthesis. Chem Catal. *1*, 1042–1054. https://doi.org/10.1016/j.checat.2021.08.006.

34. Miyahara, S.I., Sato, K., Kawano, Y., Imamura, K., Ogura, Y., Tsujimaru, K., and Nagaoka, K. (2021). Ammonia synthesis over lanthanoid oxide-supported ruthenium catalysts. Catal. Today *376*, 36–40. https://doi.org/10.1016/j.cattod.2020.08.031.

35. Dahl, S., Törnqvist, E., and Chorkendorff, I. (2000). Dissociative adsorption of N_2 on Ru(0001): A surface reaction totally dominated by steps. J. Catal. *192*, 381–390. https://doi.org/10.1006/jcat.2000.2858.

36. Kitano, M., Kujirai, J., Ogasawara, K., Matsuishi, S., Tada, T., Abe, H., Niwa, Y., and Hosono, H. (2019). Low-Temperature Synthesis of Perovskite Oxynitride-Hydrides as Ammonia Synthesis Catalysts. J. Am. Chem. Soc. *141*, 20344–20353. https://doi.org/10.1021/jacs.9b10726.

37. Gál, Z.A., Cario, L., and DiSalvo, F.J. (2003). Synthesis, structure and magnetic properties of the ternary nitride $La_3V_2N_6$. Solid State Sci. *5*, 1033–1036. https://doi.org/10.1016/s1293-2558(03)00135-3.

38. Niewa, R., Hu, Z., Grazioli, C., Rößler, U., Golden, M.S., Knupfer, M., Fink, J., Giefers, H., Wortmann, G., de Groot, F.M.F., and DiSalvo, F.J. (2002). XAS spectra of $Ce_2[MnN_3]$ at the Ce-$M_{4,5}$, Ce-L_3, Mn-$L_{2,3}$ and N-K thresholds. J. Alloys Compd. *346*, 129–133. https://doi.org/10.1016/s0925-8388(02)00519-4.

39. Tessier, F., Ranade, M.R., Navrotsky, A., Niewa, R., DiSalvo, F.J., Leineweber, A., and Jacobs, H. (2001). Thermodynamics of formation of binary and ternary nitrides in the System Ce/Mn/N. Z. Anorg. Allg. Chem. *627*, 194–200. https://doi.org/10.1002/1521-3749(200102)627:2<194::Aid-zaac194>3.0.CO;2-0.

40. Cao, B., Veith, G.M., Neuefeind, J.C., Adzic, R.R., and Khalifah, P.G. (2013). Mixed Close-Packed Cobalt Molybdenum Nitrides as Non-noble Metal Electrocatalysts for the Hydrogen Evolution Reaction. J. Am. Chem. Soc. *135*, 19186–19192. https://doi.org/10.1021/ja4081056.

41. Gregory, D.H., Hargreaves, J.S.J., and Hunter, S.M. (2011). On the regeneration of Co_3Mo_3N from Co_6Mo_6N with N_2. Catal. Lett. *141*, 22–26. https://doi.org/10.1007/s10562-010-0464-3.

STAR★METHODS

KEY RESOURCES TABLE

REAGENT or RESOURCE	SOURCE	IDENTIFIER
Chemicals, peptides, and recombinant proteins		
Eu	Beijing Ryubon New Material Technology, LTD	CAS No.: 7440-53-1
$MnCl_2$	Alfa Aesar	CAS No.: 7773-01-5
$LiNH_2$	Alfa Aesar	CAS No.: 7782-89-0
THF	Macklin	CAS No.: 109-99-9
Software and algorithms		
Origin 2021	OriginLab Corp.	https://www.originlab.com/2021
EasyDirect™ pH	Mettler Toledo	https://www.mt.com/cn/zh/home/products/lab-solutions/lab-software/easydirect.html
Other		
XRD	Panalytical	https://www.malvernpanalytical.com.cn/about-us
TEM JEM-2100	JEOL	https://www.jeol.com/corporate/globalnetwork/
SEM JSM-7800F	JEOL	https://www.jeol.com/corporate/globalnetwork/
BET Specific Surface Area	Anton Paar	https://www.anton-paar.cn/about-us/company/
X-ray photoelectron spectroscopy-ThermoFisher ESCALAB 250Xi	Thermo Fisher Scientific	https://corporate.thermofisher.com/us/en/index/about.html
Mass Spectrometer-Hiden HPR20	Hiden Analytical	https://www.hidenanalytical.com/
Mettler Toledo SevenMulti	Mettler Toledo	https://www.mt.com/cn/zh/home.html

METHOD DETAILS

Catalyst preparation

The precursor of MnN, denoted as Mn-NH, was prepared by ball-milling the mixtures of manganese chloride ($MnCl_2$, Alfa, 97%) and lithium amide ($LiNH_2$, Aldrich, 95%). MnN was obtained by calcinating the Mn-NH precursor under vacuum at 300°C for 3 h, and the LiCl by-product was removed by washing with THF for several times. EuH_2 was prepared by loading a certain amount of europium metal powder in a stainless steel reactor filled with 2.5 MPa of H_2, and heating at a ramping rate of 5 °C min^{-1} to 600°C for 36 h, then the sample was transferred into a stainless steel jar with 1.0 MPa of H_2, and ball-milled on a Retsch planetary ball mill (PM 400) at 200 rpm for 2 h. Mn_4N-EuN composite catalyst was prepared by ball-milling a certain amount of MnN and EuH_2 at 200 rpm for 3 h. Mn_4N-EuN-IM was prepared by an impregnation method, the Mn-NH was impregnated in a europium-ammonia solution, where europium metal can be converted to $Eu(NH_2)_2$, and $Eu(NH_2)_2$ can be converted to EuN after reaction under a flow of 75% H_2/N_2. Mn-NH was washed by THF to remove LiCl before impregnation.

Catalyst activity test and kinetic analysis

The ammonia synthesis performance was evaluated in a stainless-steel reactor with a WHSV of 60000 mL g^{-1} h^{-1} under the reaction conduction of 300°C–450°C under 1.0 MPa. The catalysts (30 mg) were heated from room temperature to 450 °C at a ramping rate of 5 °C min^{-1} under 75% H_2/N_2 mixture gas (30 mL min^{-1}). The ammonia production rate was measured by using a conductivity meter (Mettler Toledo SevenMulti). The exhaust gas was directed into a diluted sulfuric acid solution, and the change in proton conductivity over time was measured. Changes in conductivity were tracked using an EasyDirect pH software, and the data can be converted into a Word document. The calculation method of ammonia synthesis rate is described in the following quantification and statistical analysis section.

Reaction kinetics were performed at 350°C and 1.0 MPa NH_3 reaction order was measured by changing the gas (75% H_2-25% N_2) flow rate from 18 to 48 mL min^{-1}, and keeping a constant N_2 and H_2 partial pressure. The reaction order of H_2 was obtained at a constant flow 30 mL min^{-1} using Ar gas as a diluent, the flow gas fixed N_2 partial pressure (0.2 MPa) while changing the H_2 partial pressure from 0.2 to 0.7 MPa. Similarly, the N_2 reaction order was measured by fixing the H_2 partial pressure (0.5 MPa) while changing the N_2 partial pressure from 0.05 to 0.5 MPa, and the gas flow at a constant flow 30 mL min^{-1}.

Catalyst characterization

XRD patterns were performed on a PANalytical X'pert diffractometer using a homemade sample cell covered with KAPTON film to avoid air contamination. TEM images were obtained using a JEM-2100 electron microscope. The catalyst powder was dispersed in cyclohexane and

dropped on a carbon-coated copper TEM grid. The morphology of the sample was evaluated using field-emission scanning electron microscopy (JSM-7800F), and the component elements were analyzed using energy-dispersive X-ray spectroscopy (EDX, JSM-7800F). XPS (ThermoFisher ESCALAB 250Xi) measurements were performed using Al Kα (hν = 1486.6 eV) radiation as a trigger. Charging effects were corrected by the C1s binding energy of 284.8 eV. The BET specific surface areas of catalysts were measured by N_2 physisorption at −196°C on a Quadrasorb evo instrument. Temperature-programmed techniques were performed on a quartz-lined stainless-steel reactor and the tail gases were analyzed by an online mass spectrometer (MS, Hiden HPR20). Sample was heated in H_2 (H_2-TPR) or Ar (Ar-TPD) from room temperature to desired temperatures. N_2 isotopic exchange experiments were performed in a stainless-steel reactor connected to a vacuum-pumping system. 50 mg catalyst was loaded into the reactor in the Ar-filled glovebox. The sample was treated at 300°C, and a mixture of $^{15}N_2$ and $^{14}N_2$ ($^{15}N_2/^{14}N_2$ = 1:4.4, total pressure: 31.34 kPa) was then introduced in the stainless-steel reactor. The m/z signals at 28, 29 and 30 were monitored by a MS (HPR 20, Hiden).

QUANTIFICATION AND STATISTICAL ANALYSIS

This study includes calculations of ammonia synthesis rate, apparent activation energy, and reaction order.

Calculation of ammonia synthesis rate

The ammonia synthesis rate r_{NH3} is calculated using Equation 1:

$$r_{NH_3} = \frac{\Delta C * a * 3600}{600 * m_{cat}} \quad \text{(Equation 1)}$$

Here, ΔC represents the change in conductivity over 10 min. The coefficient a is defined as the ratio of the amount of ammonia to the change in conductivity, and m_{cat} is the weight of the catalyst.

Calculation of apparent activation energy

The apparent activation energy in this paper is calculated using the Arrhenius equation (Equation 2):

$$lnk = lnA - E_a/RT \quad \text{(Equation 2)}$$

E_a is calculated from the slope of the Arrhenius plot. The unit of E_a is kJ/mol.

Calculation of reaction order

The reaction orders with respect to NH_3, N_2, and H_2 are denoted as α, β, and γ, respectively. And the ammonia synthesis rate can be represented by Equation 3:

$$r = kP_{NH_3}^{\alpha} P_{N_2}^{\beta} P_{H_2}^{\gamma} \quad \text{(Equation 3)}$$

The equation can be transformed into Equation 4:

$$lnr = lnk + \alpha\, ln\, P_{NH_3} + \beta\, ln\, P_{N_2} + \gamma\, ln\, P_{H_2} \quad \text{(Equation 4)}$$

Here, the reaction order with respect to NH_3 can be tested by changing the flow rate of reaction gas (F), and the corresponding ammonia synthesis rate can be measured. The value of α can be obtained by plotting lnC_{NH3} versus ln(1/F), where the slope represents 1/(1-α).

The C_{NH3} the ammonia concentration can be calculated by Equation 5:

$$C_{NH_3} = \frac{r_{NH_3} * m_{cat} * V_m}{1000 * \left(F * 60 - r_{NH_3} * V_m * \frac{m_{cat}}{1000}\right)} \quad \text{(Equation 5)}$$

The V_m means the standard molar volume at room temperature, and the unit is L/mol. F is the flow rate of reaction gas, the unit is mL/min.

The reaction orders of N_2 and H_2 can be calculated by changing the partial pressure of one reactant gas while fixing the partial pressure of the other one. For example, when calculating the N_2 reaction order, the ammonia synthesis rate can be given as Equation 6:

$$lnr - \alpha\, ln\, P_{NH_3} = \left(lnk + \gamma\, ln\, P_{H_2}\right) + \beta\, ln\, P_{N_2} \quad \text{(Equation 6)}$$

The partial pressure of H_2 and the total pressure remain unchanged, the value of $lnk+\gamma lnP_{H2}$ is a constant, and the reaction order with respect to N_2 (β) can be obtained from the slop of the plot.

H_2 reaction order can be calculated in the similar method.

ADDITIONAL RESOURCES

This study does not report additional resources.